Time-resolved dose distributions to moving targets during volumetric modulated arc therapy with and without dynamic MLC tracking

Thomas Ravkilde[a)]
Department of Oncology, Aarhus University Hospital, 8000 Aarhus C, Denmark and Institute of Clinical Medicine, Aarhus University, 8200 Aarhus N, Denmark

Paul J. Keall
Radiation Physics Laboratory, Sydney Medical School, University of Sydney, NSW 2006, Australia

Cai Grau, Morten Høyer, and Per R. Poulsen
Department of Oncology, Aarhus University Hospital, 8000 Aarhus C, Denmark and Institute of Clinical Medicine, Aarhus University, 8200 Aarhus N, Denmark

(Received 23 May 2013; revised 18 September 2013; accepted for publication 2 October 2013; published 28 October 2013)

Purpose: The highly conformal doses delivered by volumetric modulated arc therapy (VMAT) may be compromised by intrafraction target motion. Although dynamic multileaf collimator (DMLC) tracking can mitigate the dosimetric impact of motion on the accumulated dose, residual errors still exist. The purpose of this study was to investigate the temporal evolution of dose errors throughout VMAT treatments delivered with and without DMLC tracking.
Methods: Tracking experiments were performed on a linear accelerator connected to prototype DMLC tracking software. A three-axis motion stage reproduced representative clinical trajectories of four lung tumors and four prostates. For each trajectory, two VMAT treatment plans (low and high modulation) were delivered with and without DMLC tracking as well as to a static phantom for reference. Dose distributions were measured continuously at 72 Hz using a dosimeter with biplanar diode arrays. During tracking, the MLC leaves were continuously refitted to the 3D target position measured by an electromagnetic transponder at 30 Hz. The dosimetric errors caused in the 32 motion experiments were quantified by a time-resolved 3%/3 mm γ-test. The erroneously exposed areas in treatment beam's eye view (BEV) caused by inadequate real-time MLC adaptation were calculated and compared with the time-resolved γ failure rates.
Results: The transient γ failure rate was on average 16.8% without tracking and 5.3% with tracking. The γ failure rate correlated well with the erroneously exposed areas in BEV (mean of Pearson $r = 0.83$, $p < 0.001$). For the final accumulated doses, the mean γ failure rate was 17.9% without tracking and 1.0% with tracking. With tracking the transient dose errors tended to cancel out resulting in the low mean γ failure rate for the accumulated doses.
Conclusions: Time-resolved measurements allow pinpointing of transient errors in dose during VMAT delivery as well as monitoring of erroneous dose evolution in key target positions. The erroneously exposed area in BEV was shown to be a good indicator of errors in the dose distribution during treatment delivery. [http://dx.doi.org/10.1118/1.4826161]

Key words: organ motion compensation, dynamic MLC tracking, dose verification, time-resolved dosimetry

1. INTRODUCTION

In radiotherapy, volumetric modulated arc therapy (VMAT) enables efficient and highly conformal dose delivery.[1–3] However, motion of the targeted tumor and surrounding organs during treatment delivery may compromise the intended dose distribution.[4] A promising method to account for the intrafraction motion is dynamic multileaf collimator (DMLC) tracking in which real-time target position monitoring is used for continuous adaptation of the planned MLC aperture to the moving target position.[5–8]

Even with DMLC tracking residual dosimetric errors exist,[9,10] mainly because the MLC leaves cannot always adapt to the ideal aperture, i.e., the planned MLC aperture shifted and scaled to the current target position in beam's eye view (BEV) of the treatment beam.[10] Inadequate MLC adaptation may be caused by errors in each of the three sequential steps of DMLC tracking: real-time estimation of the target position, fitting of the MLC aperture to the estimated target position, and leaf adjustment to the fitted MLC aperture.[10] Not adjusting for target rotation may additionally be a cause of dosimetric error.[11] Recent studies suggest dosimetric benefits of more robust treatment planning with DMLC tracking in mind[12,13] or of alternative tracking methods, such as couch tracking,[14] that are independent of the physical constraints of the MLC.

The advent of radiotherapy treatment modalities of increasing complexity has recently sparked an interest in time-resolved dosimetry. Thus, a number of methods have been

proposed for time-resolved dosimetry ranging from verification of dynamic treatments using an electronic portal imager device (EPID) (Ref. 15) over *in vivo* online error detection in brachytherapy[16] to measurement-guided 4D dose reconstruction.[17] Adding temporal resolution to dose measurements for DMLC tracking may provide better understanding of the residual dosimetric errors, which may further improve the dosimetric performance of the tracking treatments.

The purpose of this study was to investigate the evolution of the dose errors resulting from motion throughout VMAT treatments delivered both with and without DMLC tracking using time-resolved dose measurements.

2. METHODS

In this section, we will cover the experiments performed, processing and analysis of the data, and the statistical methods applied.

2.A. Experiments

Figure 1 shows the experimental setup for electromagnetic (EM) based DMLC tracking experiments with time-resolved measurements of the delivered dose distribution. The experiments were carried out on a Trilogy linear accelerator equipped with a 120 leaf Millennium MLC (Varian Medical Systems, CA). DMLC tracking was performed by prototype tracking software[6] using the real-time 3D target position signal of a wired EM transponder system (RayPilot, Micropos Medical, Sweden).[18] The 3D target position was acquired at 30 Hz and the MLC leaves were continuously adapted to the measured 3D position. For simulation of the dosimetric impact of motion of lung tumors, prediction was used to compensate for the tracking system latency, which was previously measured to be 140 ms.[18] In the current experiments, analysis of log files generated during DMLC tracking of a sinusoidal motion was used to determine the target position logging latency, i.e., the time delay from the target occupying a given position until the logging of this position by the tracking software.

A dosimeter phantom (Delta4PT, Scandidos, Sweden) (Ref. 19) with two orthogonal planar diode arrays (total of 1069 diodes) encased in cylindrical PMMA was used for time-resolved measurements of the dose delivery. The delivered *transient* dose distribution, i.e., the dose delivered in a short time interval, and the number of delivered dose pulses was measured with the dosimeter at a rate of 72 Hz. The dosimeter phantom was placed on a programmable motion stage[20] that was modified inhouse to carry the phantom.[21] The modification consisted of a custom built platform made of wood mounted on a three-axis motion stage in one end and supported by a one-axis motion stage at the other end to share the weight of the heavy phantom. Vertical phantom motion was performed by synchronous motion of the two motion stages along the vertical axis. Lateral and longitudinal phantom motion was performed by the three-axis motion stage. The platform could follow this motion unrestrictedly due to spherical wheels rolling on an aluminum plate mounted to the supporting one-axis motion stage. The dose to the dosimeter was dampened when the treatment couch, RayPilot antennae system, and/or the motion stage platform was inside the treatment beam. However, the damping was approximately identical for experiments with the same VMAT plan and was assumed to cancel out when comparing motion experiments with static reference experiments. Routine clinical quality assurance (QA) calibration of the Delta4PT phantom was performed prior to measurements.

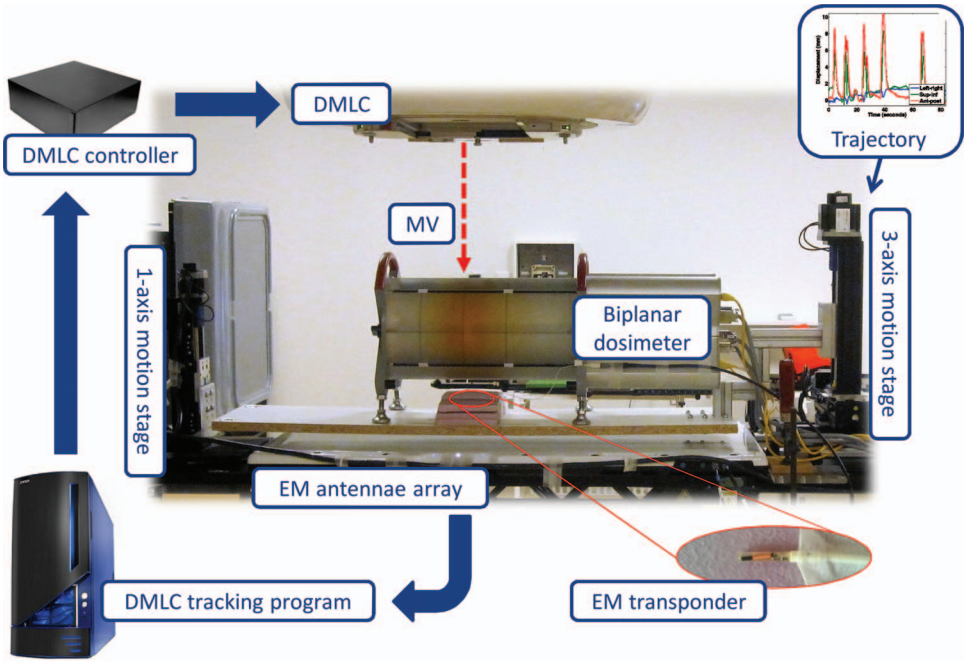

FIG. 1. Photo of the experimental setup for DMLC tracking. Tumor trajectories were reproduced by a three-axis motion stage that was modified to carry a biplanar diode arrays dosimeter with support of a vertically moving one-axis motion stage. The target position was continuously provided by a wired EM transponder system to the DMLC tracking loop. Time-resolved measurements of dose distributions were performed by the dosimeter.

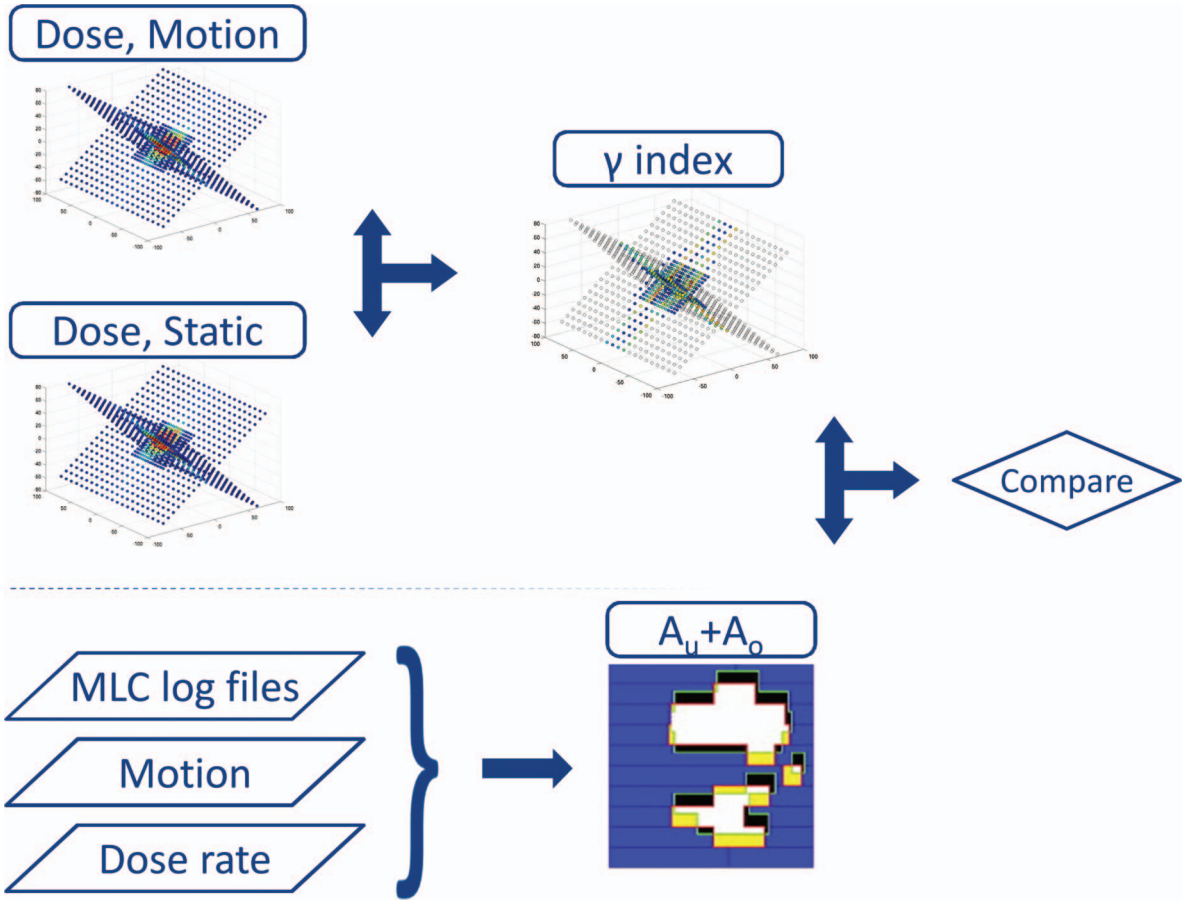

FIG. 2. Schematic representation of the data flow. At each point in time, measured doses of motion experiments with or without tracking were compared with the measured doses of the static reference by means of a 3%/3 mm γ-test. Tracking log files containing MLC and motion data were analyzed taking into account the dose rate measured by the Delta4PT phantom to construct dose rate-weighted areas of underexposure and overexposure A_u+A_o. Finally, A_u+A_o and γ failure rates were compared.

The experiments were performed with the same tumor motion trajectories and VMAT plans as used in previous studies of DMLC tracking performance.[9,10] Eight representative tumor trajectories; four lung tumors measured by a Cyberknife system[22] ("Typical case", High-frequency breathing, Predominantly left-right motion, and Baseline shifts) and four prostates measured by a Calypso EM transponder system[23] (Continuous drift, Persistent excursion, Transient excursion, and High-frequency excursions), were carefully selected from large thoracic/abdominal[24] and prostate[25] tumor motion databases as representing a set of characteristic motion patterns for these tumor sites.[9] For each trajectory, two 358° single-arc 6 MV RapidArc VMAT plans (low and high modulation) were delivered to the moving phantom in separate experiments. The collimator rotation was 90° resulting in the MLC leaves travelling along the cranio-caudal (CC) direction. The VMAT plans were delivered with modulated dose rate and gantry speed.[10] Monitor units (MU) and treatment delivery times were 342 MU and 76 s (low modulation lung plan), 596 MU and 78 s (high modulation lung plan), 422 MU and 77 s (low modulation prostate plan), and 737 MU and 84 s (high modulation prostate plan). The four VMAT plans were delivered for each of the four corresponding trajectories (lung or prostate) once with and once without DMLC tracking, as well as three times to a static phantom for reference, totaling 44 separate deliveries (four tracking, four non-tracking, and three static deliveries for each of the four VMAT plans).

2.B. Data analysis

The data analysis is summarized in Fig. 2. After completion of the experiments, Dynalog MLC log files[26] and tracking log files from the tracking program (containing MLC apertures, gantry angles, and the measured target motion) were collected and synchronized by cross correlation of gantry angles as a function of time. These log files were then synchronized to the time-resolved dosimeter data by use of the Dynalog beam-on flag. The time-resolved dosimeter data were measured using the clinical Delta4PT software and exported to plain text files using a prototype research version provided by the vendor for optimal temporal resolution.

In order to compare the time-resolved dose of motion experiments with static reference experiments, the experiments must be synchronized. To do so the number of delivered dose pulses was used as the indicator of treatment progression. For each treatment plan, the total numbers of dose pulses in the experiments were normalized to the mean total number of

dose pulses of the relevant static experiments. The number of dose pulses per sampling in the dose measurements ranged from 0 to 5. To ensure robust comparison between the experiments, the dose measurements were downsampled to equidistant steps of 10 dose pulses by linear interpolation of the *cumulative* dose, i.e., the built-up dose from start of beam delivery until the current time. The mean temporal resolution of the downsampled dose data was 50 ± 31 ms [one standard deviation (SD)], which is comparable to the temporal resolution of the Dynalog files (50 ms).

For each plan, the static reference dose was created as the mean of the three beam deliveries to the static phantom. The dose distributions delivered during motion were compared with the static reference dose distributions using a time-resolved 3%/3 mm γ-test,[27] i.e., a γ-test comparison of dose distributions was done for each point in time during treatment delivery. The time-resolved γ-test was implemented in Matlab (MathWorks Inc., MA) and was optimized specifically for the Delta4PT geometry (combined 2D γ-tests of each plane). Validation of the algorithm was done by comparing γ index maps of measured *accumulated* (total from complete beam delivery) dose distributions with the corresponding γ index maps calculated by the clinical Delta4PT software. The choice of pass criteria of 3%/3 mm was based on the extensive use of these in the literature, thus creating a large base of reference. Furthermore, 3%/3 mm γ pass criteria were also used in previous studies of DMLC tracking performance for VMAT (Refs. 9 and 10) and are routinely used for clinical VMAT QA at our clinic. The percentage dose difference in the γ-test was calculated relative to the maximum dose for each corresponding point in time in the measured static reference. Detectors with final accumulated doses below 5% of the maximum accumulated dose in the measured static reference were excluded in the calculations.

For each of the four VMAT plans, the ability of the linear accelerator to reproduce the treatment at all times during delivery to the static target was quantified by time-resolved γ-tests that compared all six pairwise combinations of the three static treatment deliveries. The γ-test failure rates with motion were calculated both for the transient, cumulative, and final accumulated dose distributions.

The ideal MLC aperture during treatments with target motion is the planned MLC aperture shifted and scaled to the current target position in BEV of the treatment beam. The deviation from this ideal aperture was determined by comparison with the actually achieved MLC aperture and current target position. In this analysis, the real-time measured target position recorded in the tracking logs (rather than the trajectory input into the motion stage) was used as the ground truth target position since the EM transponder has been proven very accurate in previous DMLC tracking experiments.[18] The deviation between the ideal and actual apertures was quantified as the erroneously underexposed area A_u and erroneously overexposed area A_o, i.e., the areas that were incorrectly outside or inside the MLC aperture, respectively[10] (see Fig. 2). The erroneously exposed areas A_u and A_o were calculated at each time point for both tracking and nontracking treatments. In the DMLC tracking experiments, A_u and A_o had contributions from insufficient MLC adaptation occurring in the three consecutive MLC adaptation steps: target localization, leaf fitting, and leaf adjustment.[10] Without tracking the main contribution to A_u and A_o was the noncompensated target motion in BEV. To account for dose rate variations, the time-resolved dose rate-weighted sum of the under- and overexposed areas (hereafter denoted A_u+A_o) was calculated using the dose rate measured by the dosimeter.

2.C. Statistical analysis

A possible linear relationship between transient γ-test failure rates and A_u+A_o was tested in Matlab by Pearson's product-moment correlation coefficient using a significance level of 5%. The assumptions for the statistical model were checked by a density histogram plot, Q-Q plots, and diagnostic plots of the residuals of a simple linear regression.

3. RESULTS

The target position logging latency of the connected EM transponder and DMLC tracking software was found to be 90 ms. The total number of dose pulses delivered to the static target for the VMAT treatment plans had a mean SD of 0.3% of the mean total number of dose pulses. The total treatment delivery time for the VMAT treatment plans was independent of DMLC tracking being applied and had a mean SD of 0.4% of the mean total treatment time. Mean time resolutions after downsampling and the spread in time resolutions due to dose rate modulation are listed in Table I. For all treatment plans, the three treatment deliveries to the static phantom resulted in total accumulated doses with 0% γ-test failure rates when compared pairwise with each other using 3%/3 mm criteria. This reproducibility was somewhat lower for the cumulative doses (mean γ-test failure rate of 0.22%) and transient doses (mean γ-test failure rate of 1.43%) as seen in Table I. The

TABLE I. Temporal resolution and reproducibility of treatments to the static phantom by the mean of time-resolved γ failure rates of final accumulated, cumulative, and transient doses in static experiments.

VMAT plan	Lung (low modulation)	Lung (high modulations)	Prostate (low modulation)	Prostate (high modulation)
Mean time resolution $\pm$ 1 SD (ms)	68 ± 19	40 ± 13	56 ± 19	35 ± 10
Accumulated (%)	0	0	0	0
Cumulative (%)	0.27	0.19	0.39	0.01
Transient (%)	1.30	1.29	2.39	0.76

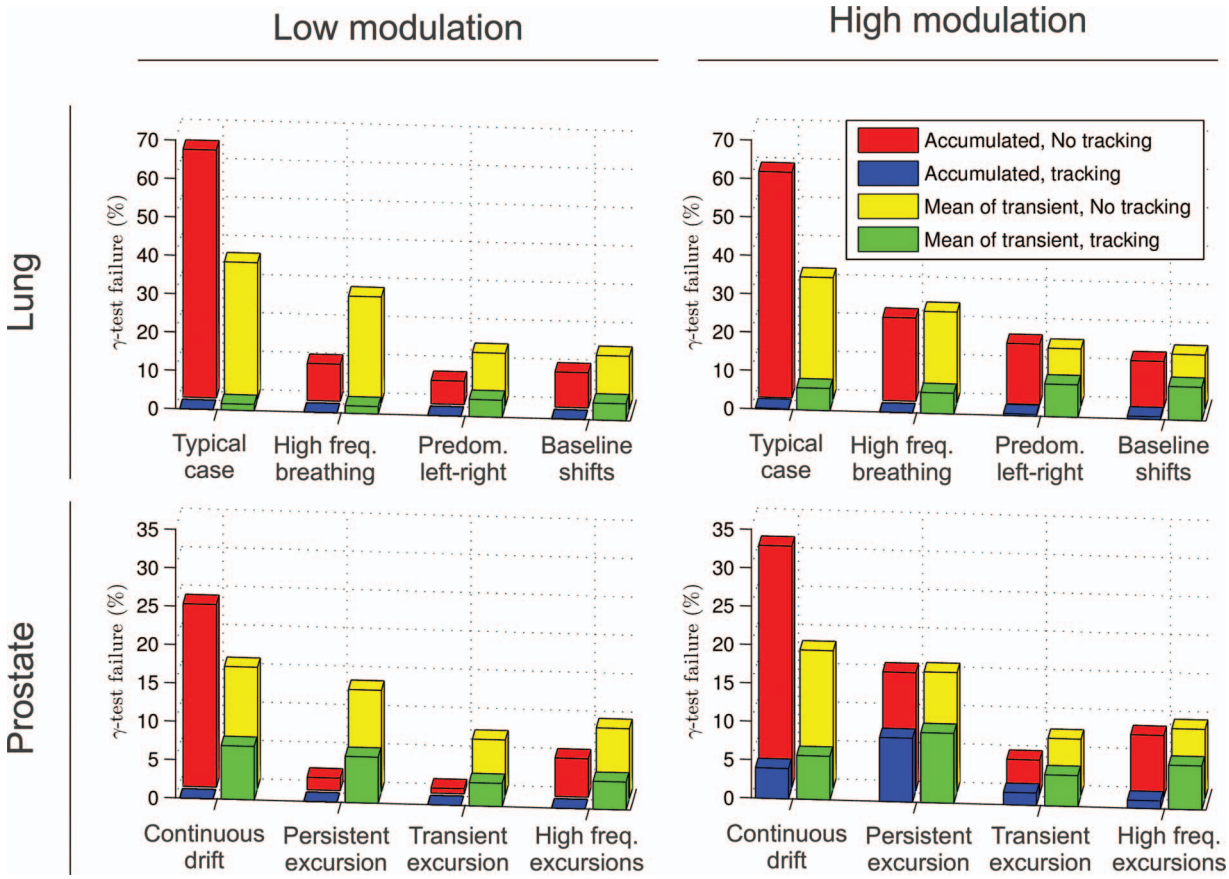

FIG. 3. Percentage of detectors failing the 3%/3 mm γ-test during VMAT without tracking (rear left bars) and with tracking (front left bars) for the four lung tumor trajectories (top) and the four prostate tumor trajectories (bottom). (Left) Low-modulation VMAT plans. (Right) High-modulation VMAT plans. Mean γ-test failure rates of transient dose distributions are also shown without tracking (rear right bars) and with tracking (front right bars). Note the different y-scales between lung and prostate tumor trajectories.

number of detectors included in the γ-tests ranged from 395 to 685 between VMAT treatment plans.

Figure 3 shows that considerable transient γ-test failures were observed during delivery both without tracking (mean of 16.8%) and with tracking (mean of 5.3%). However, tracking tended to mitigate the systematic component of erroneous delivery allowing residual errors to cancel out. Thus, the mean γ failure rate of final accumulated doses dropped from 17.9% without tracking to 1.0% with tracking. Only for the high modulation prostate plan were the errors in final accumulated dose considerably different from zero. The mitigation by tracking of the systematic component of erroneous dose delivery is visualized by the dose to a single detector with and without tracking in the example in Fig. 4.

The time-resolved results of the deliveries of the two high modulation treatment plans are shown in Figs. 5 and 6. Inspecting rows A-C for nontracking experiments in each of Figs. 5 and 6 immediately shows a strong resemblance between the 2D displacement of the target as seen in BEV of the treatment beam, the A_u+A_o, and the transient γ failure rate. For tracking treatments, there is still large similarity between A_u+A_o and the transient γ failure rates (note, for instance, the peaks at the abrupt target position shifts in the transient excursion prostate trajectory in Fig. 6), while the similarity

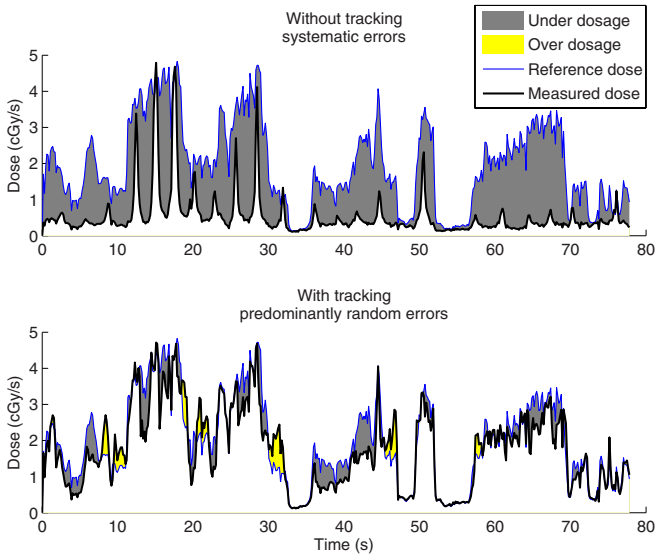

FIG. 4. Transient absorbed doses in one sample detector for the high-modulated lung VMAT plan delivered to the phantom reproducing the "Typical case" lung trajectory without tracking (top) and with tracking (bottom). This lung trajectory displays a systematic position shift. The reference dose to the static phantom (thin line) is the same in both plots. The doses measured in either tracking or nontracking treatments to the moving phantom are shown as thick lines. Resulting transient underdosage and overdosage are visualized by areas.

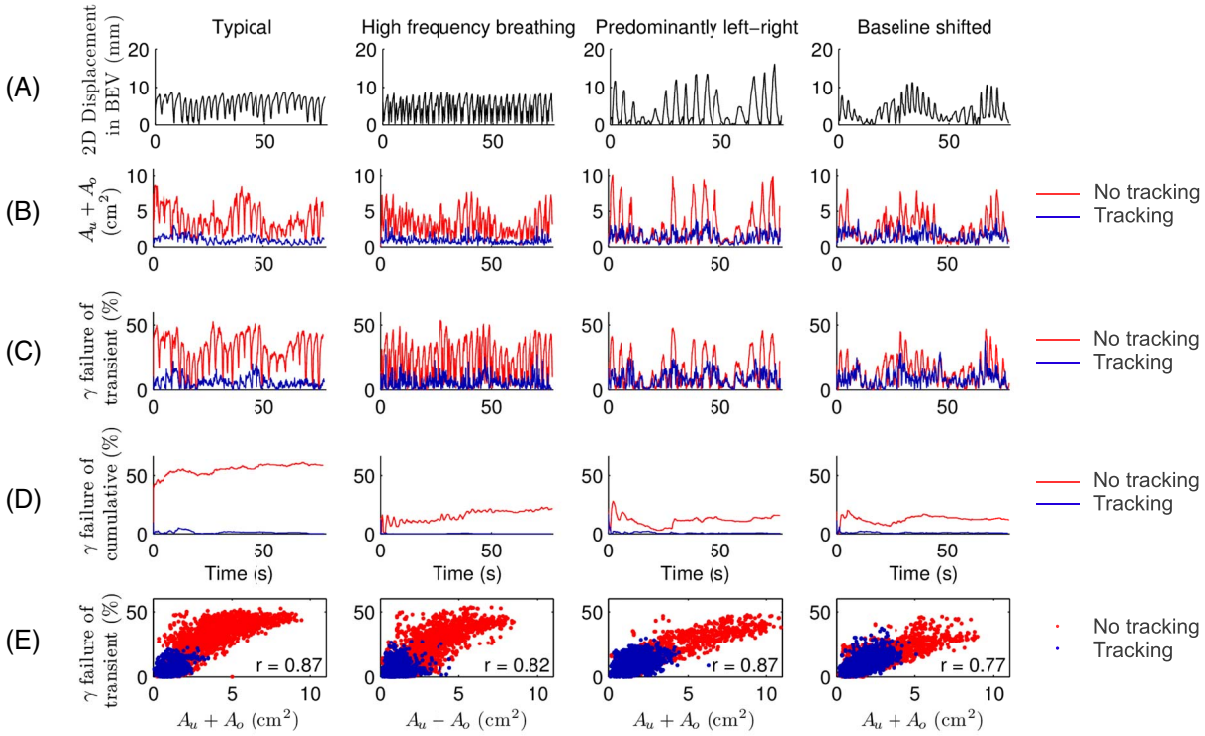

FIG. 5. Comparison of target motion, exposure errors, and dosimetric errors during the high modulation VMAT deliveries for the four lung trajectories. Row A: absolute 2D displacement of the target from the origin in BEV of the treatment beam. Rows B-D: transient dose rate-weighted sum of erroneously underexposed and overexposed areas A_u+A_o (B), γ-test failure rate of transient doses (C), and γ-test failure rate of cumulative doses (D) for deliveries with and without tracking. Row E: scatter plots of γ-test failure rates of transient doses versus A_u+A_o (i.e. row C versus row B) with and without tracking. The Pearson linear correlation coefficient r is listed for each scatter plot.

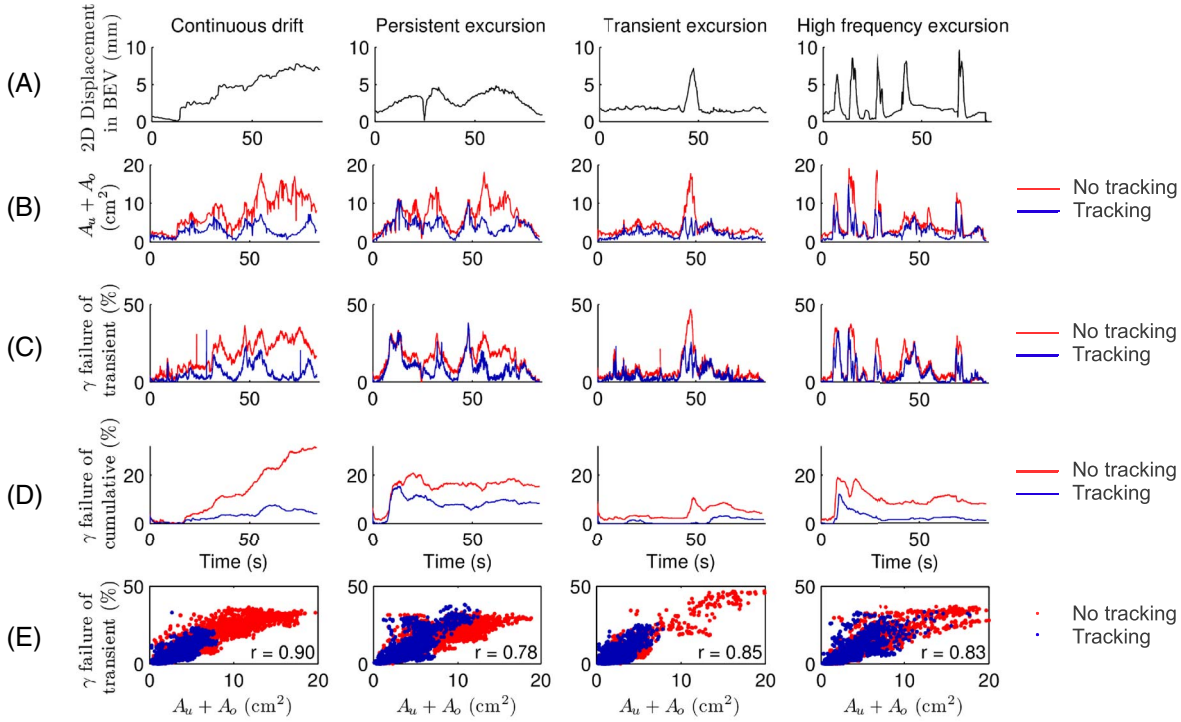

FIG. 6. Comparison of target motion, exposure errors, and dosimetric errors during the high modulation VMAT deliveries for the four prostate trajectories. Row A: absolute 2D displacement of the target from the origin in BEV of the treatment beam. Rows B-D: transient dose rate-weighted sum of erroneously underexposed and overexposed areas A_u+A_o (B), γ-test failure rate of transient doses (C), and γ-test failure rate of cumulative doses (D) for deliveries with and without tracking. Row E: scatter plots of γ-test failure rates of transient doses versus A_u+A_o (i.e. row C versus row B) with and without tracking. The Pearson linear correlation coefficient r is listed for each scatter plot.

with the BEV motion trajectory is less obvious. This is because the displacement in BEV is compensated for by MLC adaptation, and A_u+A_o and the transient γ failure rate instead reflect the residual tracking error. The γ-test failure rates of cumulative doses (row D in Figs. 5 and 6) to some extent reflect A_u+A_o (row B) at start of treatment, but the resemblance disappears 10–20 s into the treatment. The γ-test failure rates of cumulative doses also show how erroneous treatment delivery may be compensated during the remainder of the treatment, e.g., prostate high frequency excursions in Fig. 6. The strong correlation between A_u+A_o and transient γ-test failure rates at any point in time during treatment delivery is further visualized by the scatter plots in row E of Figs. 5 and 6. The mean of correlation coefficients across all VMAT treatment plans and tumor trajectories was $r = 0.83$ including both tracking and nontracking treatments, indicating strong linear correlation between A_u+A_o and transient γ failure. The correlation was highly statistically significant ($p < 0.001$) in all cases.

4. DISCUSSION

Measurements of dose distributions with high temporal resolution were demonstrated for VMAT treatments with and without DMLC tracking, clearly illustrating transient motion induced errors in the delivered dose distributions. Errors in transient doses can be measured independently of the linear accelerator using the technique for time-resolved measurements of dose distributions developed for this study and utilized to pinpoint transient errors in beam delivery. This technique is not limited to tracking treatments and is readily applicable for nonclinical employment such as phantom studies and machine QA.

High reproducibility of transient and cumulative dose distributions is of course imperative for the credibility of the results in the present study. The treatment was shown to be very reproducible for transient, cumulative, and final accumulated doses during delivery. The mean γ failure rates of transient dose distributions for treatment deliveries to static phantoms represent lower bounds for the γ failure rates achievable with perfect tracking. The numbers of detectors included in the γ-tests were several hundred for every VMAT treatment plan, thus providing an acceptable data quantity for the γ-tests.

DMLC tracking based on a wired EM target localization system was applied to amend erroneous delivery of dose distributions due to motion. While DMLC tracking greatly improved treatment delivery, large residual errors still existed in the transient dose. Transient errors tended to cancel out in the final accumulated dose for most VMAT deliveries, however, leaving substantial accumulated dose errors present only for tracking of the high modulation prostate plan delivered with the relatively slow prostate motions of the continuous drift and persistent excursion trajectories (Fig. 3). For prostate motion, leaf fitting has previously been shown to be the dominant error contributor for DMLC tracking.[10] If the target moves perpendicular to the MLC leaves, the leaf fitting cannot be made without errors. For high frequency motion, the resulting transient dosimetric errors will tend to cancel out whereas they may build up for slower motion, where the target may stay shifted in the same direction for considerable periods of time, leading to systematic dose errors. This is probably the reason for the larger residual accumulated dose errors for the slow prostate trajectories when tracked with the high modulation VMAT plan. The results suggest that thinner MLC leaves, or restraints on the level of plan modulation, could improve the tracking. Alternatively, methods of target tracking that do not involve leaf fitting or leaf adjustment in the beam-target realignment, such as gimbal tracking[28] or couch tracking,[14] could be used.

The γ-test failure rates of accumulated doses in Fig. 3 are similar to, but generally somewhat lower than, those reported in two earlier studies of other types of DMLC tracking with the same tumor motion trajectories and VMAT plans.[9,10] Those studies both used a PTW ion chamber array, which has a lower resolution than the dosimeter used in the present study. In both studies, the dosimeter was also placed in a horizontal plane rather than the present biplanar diagonal configuration. Thus, different parts of the dose distribution have essentially been measured. The lower γ failure rates may also be due to the lower latency of the real-time target localization system used in the present study, or it may be caused by differences in the sections of the tumor trajectories that were used. Different combinations of motion and apertures will yield different interplay effects. The spread in this uncertainty was not investigated since only one tracking and one nontracking measurement was performed per trajectory for each VMAT plan. The demonstrated link between BEV target displacements, A_u+A_o, and transient γ-test failure rates is, however, likely to hold independent of the trajectory sections used for the experiments. The present γ-test results have been validated by the highly modulated VMAT lung plans being delivered twice with comparable results and by the results of our own γ-test being compared with results from the γ-test in the clinical Delta4PT software.

There was good linear correlation between A_u+A_o and γ-test failure rates of transient doses. Good correlation has previously been demonstrated between the mean of A_u+A_o during treatment and the γ failure rate of the final accumulated dose distribution.[10] Here, we have shown that A_u+A_o are a good surrogate for the level of the γ failure rate of transient dose at any point in time during treatment delivery. Since A_u+A_o can be calculated in real time, it allows intrafraction monitoring of an indicator of dosimetric accuracy of the tracking and nontracking treatment delivery. This in turn allows for correction strategies such as instant beam holds similar to conventional gating scenarios. For fixed gantry beams, the target dose distribution is approximately proportional to the 2D fluence that the beam delivers to the moving target. In such cases, keeping track of A_u and A_o during a treatment will also be able to indicate cumulative dose errors. Unfortunately, A_u and A_o cannot reconstruct how transient errors in dose build up or cancel out for treatments with beams with multiple gantry angles, such as arc treatments. In such cases, cumulation of dose errors requires a full 3D dose calculation.

5. CONCLUSIONS

Measurements of dose distributions with high temporal resolution were demonstrated for VMAT treatments with and without DMLC tracking. Transient errors in dose distributions during VMAT treatment delivery due to motion were thus rendered visible. DMLC tracking greatly improved the final accumulated dose distributions to moving targets, although large transient errors were yet found to exist. The transient errors tended to cancel out with tracking leaving only small accumulated dose errors. The time-resolved measurements allow pinpointing of transient errors in dose delivery as well as monitoring of erroneous dose evolution in key target positions. The erroneously exposed areas A_u+A_o were shown to be a good indicator for transient dose errors that can be monitored in real time during treatment.

ACKNOWLEDGMENTS

The authors gratefully thank Dr. Patrick Kupelian (University of California, Los Angeles) and Dr. Katja Langen (University of Maryland) for the prostate trajectories, Dr. Yelin Suh (MD Anderson Cancer Center) and Dr. Sonja Dieterich (University of California, Davis) for the lung tumor trajectories, Gørgen Nilsson and Peter Münger (Scandidos) for modifications of the Delta4PT software to allow export of highly time-resolved dose data, and Roman Iustin and Andreas Bergqvist (Micropos Medical AB) for modifications of the RayPilot system to allow integration with the tracking program. This work was supported by NCI Grant No. R01CA93626 and by The Danish Cancer Society, CIRRO (The Lundbeck Foundation Center for Interventional Research in Radiation Oncology), The Danish Council for Strategic Research, and Varian Medical Systems.

[a]Author to whom correspondence should be addressed. Electronic mail: thomas.ravkilde@rm.dk

[1]C. X. Yu, "Intensity-modulated arc therapy with dynamic multileaf collimation: An alternative to tomotherapy," Phys. Med. Biol. **40**(9), 1435–1449 (1995).
[2]K. Otto, "Volumetric modulated arc therapy: IMRT in a single gantry arc," Med. Phys. **35**(1), 310–317 (2008).
[3]C. Wang, S. Luan, G. Tang, D. Z. Chen, M. A. Earl, and C. X. Yu, "Arc-modulated radiation therapy (AMRT): A single-arc form of intensity-modulated arc therapy," Phys. Med. Biol. **53**(22), 6291–6303 (2008).
[4]P. J. Keall *et al.*, "The management of respiratory motion in radiation oncology report of AAPM Task Group 76," Med. Phys. **33**(10), 3874–3900 (2006).
[5]P. J. Keall, V. R. Kini, S. S. Vedam, and R. Mohan, "Motion adaptive x-ray therapy: A feasibility study," Phys. Med. Biol. **46**(1), 1–10 (2001).
[6]A. Sawant *et al.*, "Management of three-dimensional intrafraction motion through real-time DMLC tracking," Med. Phys. **35**(5), 2050–2061 (2008).
[7]Y. Liu, C. Shi, B. Lin, C. S. Ha, and N. Papanikolaou, "Delivery of four-dimensional radiotherapy with TrackBeam for moving target using an AccuKnife dual-layer MLC: Dynamic phantoms study," J. Appl. Clin. Med. Phys. **10**(2), 2926–2946 (2009).
[8]A. Krauss, S. Nill, M. Tacke, and U. Oelfke, "Electromagnetic real-time tumor position monitoring and dynamic multileaf collimator tracking using a Siemens 160 MLC: Geometric and dosimetric accuracy of an integrated system," Int. J. Radiat. Oncol., Biol., Phys. **79**(2), 579–587 (2011).
[9]P. J. Keall *et al.*, "Electromagnetic-guided dynamic multileaf collimator tracking enables motion management for intensity-modulated arc therapy," Int. J. Radiat. Oncol., Biol., Phys. **79**(1), 312–320 (2011).
[10]P. R. Poulsen, W. Fledelius, B. Cho, and P. Keall, "Image-based dynamic multileaf collimator tracking of moving targets during intensity-modulated arc therapy," Int. J. Radiat. Oncol., Biol., Phys. **83**(2), e265–e271 (2012).
[11]J. Wu *et al.*, "Electromagnetic detection and real-time DMLC adaptation to target rotation during radiotherapy," Int. J. Radiat. Oncol., Biol. Phys. **82**(3), e545–e553 (2012).
[12]M. Falk *et al.*, "The dosimetric impact of inversely optimized arc radiotherapy plan modulation for real-time dynamic MLC tracking delivery," Med. Phys. **39**(3), 1588–1594 (2012).
[13]T. Pommer *et al.*, "Dosimetric benefit of DMLC tracking for conventional and sub-volume boosted prostate intensity-modulated arc radiotherapy," Phys. Med. Biol. **58**(7), 2349–2361 (2013).
[14]M. J. Menten *et al.*, "Comparison of a multileaf collimator tracking system and a robotic treatment couch tracking system for organ motion compensation during radiotherapy," Med. Phys. **39**(11), 7032–7041 (2012).
[15]B. M. C. McCurdy and P. B. Greer, "Dosimetric properties of an amorphous-silicon EPID used in continuous acquisition mode for application to dynamic and arc IMRT," Med. Phys. **36**(7), 3028–3039 (2009).
[16]C. E. Andersen, S. K. Nielsen, J. C. Lindegaard, and K. Tanderup, "Time-resolved *in vivo* luminescence dosimetry for online error detection in pulsed dose-rate brachytherapy," Med. Phys. **36**(11), 5033–5043 (2009).
[17]B. E. Nelms *et al.*, "VMAT QA: Measurement-guided 4D dose reconstruction on a patient," Med. Phys. **39**(7), 4228–4238 (2012).
[18]T. Ravkilde, P. J. Keall, K. Højbjerre, W. Fledelius, E. Worm, and P. R. Poulsen, "Geometric accuracy of dynamic MLC tracking with an implantable wired electromagnetic transponder," Acta Oncol. **50**(6), 944–951 (2011).
[19]S. Korreman, J. Medin, and F. Kjær-Kristoffersen, "Dosimetric verification of RapidArc treatment delivery," Acta Oncol. **48**(2), 185–191 (2009).
[20]K. Malinowski *et al.*, "Development of the 4D phantom for patient-specific, end-to-end radiation therapy QA," Proc. SPIE **6510**, 65100E (2007).
[21]T. Ravkilde, P. J. Keall, C. Grau, M. Høyer, and P. R. Poulsen, "Time-resolved dose reconstruction by motion encoding of volumetric modulated arc therapy fields delivered with and without dynamic multi-leaf collimator tracking," Acta Oncol. **52**(7), 1497–1503 (2013).
[22]J. R. Adler, Jr., S. D. Chang, M. J. Murphy, J. Doty, P. Geis, and S. L. Hancock, "The Cyberknife: A frameless robotic system for radiosurgery," Stereotact. Funct. Neurosurg. **69**(1–4 Pt 2), 124–128 (1997).
[23]T. R. Willoughby *et al.*, "Target localization and real-time tracking using the Calypso 4D localization system in patients with localized prostate cancer," Int. J. Radiat. Oncol., Biol., Phys. **65**(2), 528–534 (2006).
[24]Y. Suh, S. Dieterich, B. Cho, and P. J. Keall, "An analysis of thoracic and abdominal tumour motion for stereotactic body radiotherapy patients," Phys. Med. Biol. **53**(13), 3623–3640 (2008).
[25]K. M. Langen *et al.*, "Observations on real-time prostate gland motion using electromagnetic tracking," Int. J. Radiat. Oncol., Biol., Phys. **71**(4), 1084–1090 (2008).
[26]D. W. Litzenberg, J. M. Moran, and B. A. Fraass, "Verification of dynamic and segmental IMRT delivery by dynamic log file analysis," J. Appl. Clin. Med. Phys. **3**(2), 63–72 (2002).
[27]D. A. Low, W. B. Harms, S. Mutic, and J. A. Purdy, "A technique for the quantitative evaluation of dose distributions," Med. Phys. **25**(5), 656–661 (1998).
[28]T. Depuydt *et al.*, "Geometric accuracy of a novel gimbals based radiation therapy tumor tracking system," Radiother. Oncol. **98**(3), 365–372 (2011).